A two-scale Langevin PDF model for Richtmyer–Meshkov turbulence with a small Atwood number

Olivier Soulard, Florian Guillois, Jérôme Griffond, Vladimir Sabelnikov, Serge Simoëns

Version of Record: https://www.sciencedirect.com/science/article/pii/S0167278919303720
Manuscript_1ae3c3aa40793c232c701613d13a119a

A two-scale Langevin PDF model for Richtmyer–Meshkov turbulence with a small Atwood number

Olivier Soulard[a,*], Florian Guillois[a], Jérôme Griffond[a], Vladimir Sabelnikov[b], Serge Simoëns[c]

[a] *CEA, DAM, DIF, F-91297 Arpajon, France*
[b] *ONERA, DMPE, Palaiseau, France*
[c] *École Centrale de Lyon, MFAE/LMFA, Écully, France*

Abstract

In this article, we derive a Langevin probability density function (PDF) model in order to predict turbulent mixing zone evolutions when generated by the Richtmyer–Meshkov instability. The aim of the model is to account for the permanence of large eddies which is observed in these flows when the density contrast, as measured by the Atwood number, is small. To this end, a two-scale decomposition of the velocity field is proposed and used to adapt existing Langevin models. In addition, the role played by pressure fluctuations on the transport of kinetic energy is also discussed. A closure for this turbulent process is added to the two-scale Langevin model. Finally, large-eddy simulations of Richtmyer–Meshkov turbulent flows are performed and used to validate the different closures proposed in this work.

Keywords: turbulence, probability density function (PDF), Langevin model, Richtmyer-Meshkov instability, permanence of large-eddies, pressure-velocity correlation

1. Introduction

The Richtmyer–Meshkov instability occurs when a shock wave crosses an interface separating two fluids of different densities [1–5]. Following the shock impact, perturbations initially distorting the interface grow until a mixing zone is formed and reaches a turbulent state. Meanwhile, provided the initial contrast of density is small, compressibility effects due to the shock passage decrease until the Boussinesq approximation applies and the flow becomes divergence-free [6, 7]. At large times, this incompressible turbulent mixing zone is expected to become self-similar [3–5], with the growth of the mixing zone width obeying a power law. The exponent of this law is a key parameter of Richtmyer–Meshkov turbulence [3–5].

Among the main features of small Atwood Richtmyer–Meshkov turbulence is the existence of large scale invariants of the velocity field [8–13]. The principle of permanence of large eddies applies to the flow as it does for decaying homogeneous anisotropic turbulence (HAT) [14–25]. As a result, the self-similar state of small Atwood Richtmyer–Meshkov turbulence depends on large scale initial conditions. In particular, the growth exponent of the mixing zone width can be expressed as a function of the power law exponent of the velocity spectrum at small wave numbers, called infrared exponent and denoted by s_0. Another important aspect linked to the permanence of large eddies is that the return to isotropy of the flow is only partial: large scales indeed keep their initial anisotropy. The overall anisotropy of the Reynolds stress tensor also depends on s_0.

These properties explain why applying a probability density function (PDF) model to Richtmyer–Meshkov turbulence is a challenging task. PDF models are engineering turbulence model attempting to capture the whole one-point statistical information of the velocity field and of other quantities governing the flow [26, 27]. One of the most widely used model is the Langevin PDF model, either in its simplified form (SLM) or in one of its generalized expression (GLM) [28]. The Langevin model allows to capture the statistics of a wide variety of turbulent flows, while keeping a simple and computationally efficient form. However, if applied straightforwardly to Richtmyer–Meshkov turbulent mixing zones, the Langevin model will face several issues. Indeed, it does not include any dependency on large scale initial conditions and will not be able to reproduce the different self-similar states stemming from different initial conditions. Besides, most of the existing variants of the Langevin model predict a full return to isotropy while only a partial one is expected for Richtmyer–Meshkov turbulence.

Another aspect of Richtmyer–Meshkov turbulence impedes a proper and direct application of existing Langevin models. When looking at the evolution of the turbulent kinetic energy, only three processes are active in Richtmyer–Meshkov turbulence: dissipation, turbulent advection and turbulent transport by the pressure flux. The first two are accounted for in Langevin models, with the second one being treated exactly. However, the last one, transport by

*Corresponding author
Email address: olivier.soulard@cea.fr (Olivier Soulard)

the pressure flux is almost always neglected. In all the work devoted to PDF modeling, only Ref. [29] detailed a model for the pressure flux, in order to simulate a free shear layer. In their approach, the pressure flux is modeled as an added force displacing particles along the kinetic energy gradient. While physically sound, this model does not yield a transport term in the form of the divergence of a flux. The conservation of energy on the domain cannot be ensured, which limits the applicability of this model. Setting this model aside, the neglect of the pressure flux might be appropriate in some cases [30], but it cannot be justified for Richtmyer–Meshkov turbulent flows. Indeed, dissipation and turbulent transport have orders of magnitude comparable to the pressure flux term. Therefore, in their current formulation, Langevin models do not account for an important aspect of the kinetic energy evolution in Richtmyer–Meshkov turbulence.

Thus, the purpose of this work is to derive a Langevin PDF model accounting for large scale initial conditions, partial return to isotropy and transport by the pressure flux within the framework of Richtmyer–Meshkov turbulence. To this end, we will introduce a two-scale decomposition of the PDF Langevin model, in the spirit of two-scale turbulence models such as those proposed in Refs. [31, 32]. Other multiscale PDF models already exist [33]. However, they require an additional layer of complexity we would like to avoid in the final expression of our model. Besides, they do not deal with the idea of permanence of large scales and its implications, but rather on the properties of small inertial scales. The proposed two-scale decomposition will allow to differentiate the evolutions of large permanent scales from smaller ones. As for transport by the pressure flux, we will consider the correspondence existing between Langevin PDF models and Reynolds stress models (RSM). Since explicit closures for transport by the pressure flux exist for RSM, we will propose a way to adapt them to the PDF context.

The remaining of this text is organized as follows. First, in Sec. 2, we will recall several aspects of the Richtmyer–Meshkov phenomenology. Second, in Sec. 3, we will present existing Langevin models and indicate why their formulation is insufficient for reproducing Richtmyer–Meshkov phenomenology. In Sec. 4, we will introduce a modified version of the Langevin model based on a two-scale decomposition. The adaptation of the model to account for transport by the pressure flux will be discussed in Sec. 5. Finally, the proposed model will compared against simulations in Sec. 6.

2. Phenomenology of Richtmyer–Meshkov turbulent mixing zones

Before discussing the application of a Langevin PDF model to Richtmyer–Meshkov turbulent mixing zones, we would like to recall some aspects of their phenomenology. In particular, we would like to insist on the role played by large scales on the self-similarity of the flow and on its anisotropy.

2.1. Governing equations

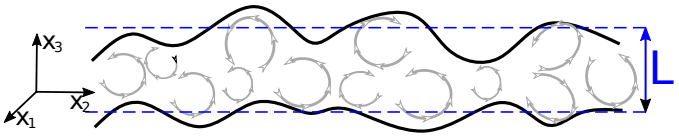

Figure 1: Schematic representation of the mixing zone.

As shown in Fig. 1, we consider a Richtmyer–Meshkov turbulent mixing zone of size L extending in the inhomogeneous direction x_3. The flow has a small Atwood number: $\mathtt{A}_t = (\rho_h - \rho_l)/(\rho_h + \rho_l) \ll 1$, with ρ_h and ρ_l the respective densities of the "heavy" and "light" fluids which are being mixed. We assume that the shock which created the mixing zone is sufficiently far in order for the flow to obey the Boussinesq approximation [6, 7]. A consequence of this approximation is that the flow is defined by an incompressible velocity field $\boldsymbol{u}$ and by the concentration c of one of the fluids being mixed. What is more, since there is no mean acceleration, the evolution of the velocity field $\boldsymbol{u}$ is independent from the concentration field c. For the sake of simplicity, we will focus in this study on the sole velocity field and on its statistics, while we will leave aside all questions regarding the concentration.

With these clarifications, and if for any given quantity q, $\overline{q}$ refers to its ensemble mean and q' to its fluctuation, the evolution of the velocity field $\boldsymbol{u}$ in Richtmyer–Meshkov turbulence is given by:

$$\partial_t u_i' + u_j' \partial_j u_i' = -\partial_i p' + \nu \partial_{jj}^2 u_i' + \partial_3 \overline{u_3'^2} \delta_{i3} \ , \tag{1a}$$

$$\partial_j u_j' = 0 \ , \ \overline{u}_i = 0 \ , \tag{1b}$$

where p is the reduced pressure and ν a molecular transport coefficient. The condition $\overline{\boldsymbol{u}} = 0$ comes from the axisymmetry of the flow and the incompressibility of the mean velocity which sets $\partial_3 \overline{u}_3 = 0$. Because $\overline{\boldsymbol{u}} = 0$, one has $\boldsymbol{u} = \boldsymbol{u}'$. We will hereafter use the notation $\boldsymbol{u}$ keeping in mind that it is really a fluctuation which we are investigating.

2.2. Self-similar turbulent state

At large times and for high Reynolds numbers, Richtmyer–Meshkov turbulent mixing zones governed by Eq. (1) reach a self-similar state. This state is usually observed and described for the mixing zone width L and for the Reynolds stress tensor $\overline{\boldsymbol{R}}$. The latter quantity is defined as:

$$\overline{R}_{ij}(x_3, t) = \overline{u_i u_j}(x_3, t) \, .$$

The trace of $\overline{\boldsymbol{R}}$ yields the turbulent kinetic energy:

$$\overline{k}(x_3, t) = \frac{1}{2} \overline{R}_{ii}(x_3, t) \, .$$

In the self-similar turbulent regime, L and $\overline{\boldsymbol{R}}$ evolve as power laws of time [3–5]:

$$L \propto t^{\Theta} \quad \text{and} \quad \langle \overline{\boldsymbol{R}} \rangle \propto t^{-2(1-\Theta)} \ , \tag{2}$$

with Θ the growth rate exponent of the mixing zone width, and $\langle \cdot \rangle$ the averaged value over the inhomogeneous direction:

$$\langle \cdot \rangle = \frac{1}{L} \int \cdot \, \mathrm{d}x_3 \, .$$

In simulations and experiments, the value of Θ has been found to vary between 0.23 to almost 2/3. As will be explained below, this value is tied to initial conditions through the principle of permanence of large scales.

Another aspect of self-similarity concerns anisotropy. Since all the components of $\langle \overline{\boldsymbol{R}} \rangle$ have the same time evolution, the anisotropy tensor based on $\langle \overline{\boldsymbol{R}} \rangle$ tends to a constant. This global anisotropy tensor is denoted by $\boldsymbol{b^G}$ and is usually different from the local anisotropy tensor $\boldsymbol{b}$ based on $\boldsymbol{R}$ or its integrated value. Both tensors $\boldsymbol{b^G}$ and $\boldsymbol{b}$ are defined as:

$$\begin{aligned} b_{ij}^G(t) =& \frac{\langle \overline{R}_{ij} \rangle}{2\langle \overline{k} \rangle}(t) - \frac{1}{3}\delta_{ij} \\ \text{and} \quad b_{ij}(x_3,t) =& \frac{\overline{R}_{ij}}{2\overline{k}}(x_3,t) - \frac{1}{3}\delta_{ij} \, . \end{aligned} \tag{3}$$

Usually, $\boldsymbol{b^G} \neq \langle \boldsymbol{b} \rangle$. Since the flow is axisymmetric, $\boldsymbol{b^G}$ is diagonal and has only one independent component. We will focus on b_{33}^G, knowing that: $b_{11}^G(t) = b_{22}^G(t) = -b_{33}^G(t)/2$. A similar relation holds for $\boldsymbol{b}$. Self-similarity implies that:

$$b_{33}^G(t) \equiv \mathrm{Cst} \, .$$

The constant value of b_{33}^G is again linked to initial conditions and in particular to the value of s_0. But, in order to explain this link, we must first give some details about the permanence of large eddies.

2.3. On the permanence of large scales

The permanence of large scales plays an important role in small Atwood Richtmyer–Meshkov turbulence. This role has been discussed in several studies [8–13] and has been verified using large-eddy simulations in [13]. The permanence of large eddies can be expressed by introducing the turbulent angular spectrum of the velocity field $E_{ij}(\boldsymbol{\kappa},t)$ at wave vector $\boldsymbol{\kappa}$:

$$\begin{aligned} & E_{ij}(\boldsymbol{\kappa},t)\delta(\kappa_1' - \kappa_1)\delta(\kappa_2' - \kappa_2) \\ =& \frac{1}{2}\left(\overline{\widehat{u}_i(\boldsymbol{\kappa},t)\widehat{u}_j^*(\boldsymbol{\kappa}',t)} + \overline{\widehat{u}_j(\boldsymbol{\kappa},t)\widehat{u}_i^*(\boldsymbol{\kappa}',t)} \right) \\ & \text{with} \quad \boldsymbol{\kappa}' = (\kappa_1', \kappa_2', \kappa_3) \\ & \text{and} \quad \widehat{u}_i(\boldsymbol{\kappa},t) = \frac{1}{(2\pi)^3} \int e^{-\imath \boldsymbol{\kappa}\cdot\boldsymbol{x}} u_i(\boldsymbol{x},t) \mathrm{d}\boldsymbol{x} \, . \end{aligned} \tag{4}$$

This spectrum is connected to the Reynolds stress tensor by the relation:

$$\langle \overline{R}_{ij} \rangle(t) = \frac{2\pi}{L} \int E_{ij}(\boldsymbol{\kappa},t) \mathrm{d}\boldsymbol{\kappa} \, . \tag{5}$$

Now, for the sake of simplicity, let us assume that the velocity spectrum generated just after the shock passage, at $t = 0$, obeys a power law:

$$E_{ij}(\boldsymbol{\kappa}, t=0) = E_{ij}^{(0)}(\boldsymbol{\kappa}) \propto \kappa^{s_0 - 2} \quad \text{for } \kappa \ll \kappa_{\ell_0} \ ,$$

with $\kappa = \sqrt{\kappa_i \kappa_i}$ the modulus of the wavevector $\boldsymbol{\kappa}$ and $\kappa_{\ell 0}$ the wave number associated with the initial value ℓ_0 of the integral scale $\ell(t)$. Then, the principle of permanence of large eddies states that for scales much larger than the integral scale of turbulence $\ell(t)$ and for $s_0 < 4$, E_{ij} remains constant:

$$\begin{aligned} \text{For } \kappa \ll \kappa_\ell(t) = {}^{2\pi}/_{\ell(t)} \quad \text{and} \quad s_0 < 4 \ , \\ E_{ij}(\boldsymbol{\kappa},t) = E_{ij}^{(0)}(\boldsymbol{\kappa}) \propto \kappa^{s_0-2} \ , \end{aligned} \tag{6}$$

The integral scale of turbulence ℓ is representative of energy containing eddies and is usually on the order of $L/3$ to $L/2$. Note that the spectrum $\boldsymbol{E}$ is proportional to k^{s_0-2} and not k^{s_0} because it is an angular spectrum and not a modulus spectrum. Note also that the limit exponent $s_0 = 4$ arises because non-linear effects become predominant when $s_0 > 4$ and impede the preservation of initial conditions [13].

Because initial conditions are preserved at large scales, they constrain the self-similar behavior of the flow. Indeed, if the spectrum is to be self-similar and permanent at large scales, then a large scale invariant must exist. This invariant can be expressed as [13]:

$$\langle \overline{k} \rangle L^{s_0+2} = \mathrm{Cst} \, . \tag{7}$$

From this relation, one can show that the characteristic exponent of the self-similar state of Richtmyer–Meshkov turbulence is directly linked to the infrared exponent s_0:

$$\Theta = \frac{2}{s_0 + 4} \, . \tag{8}$$

The smaller s_0 is, the larger the contribution of large scales is and the faster the growth of the mixing zone width is. The value of Θ varies from 0.25 for $s_0 = 4$ to 0.5 for $s_0 = 0$. Note that Θ cannot exceed 2/3 as discussed in [34, 35].

The invariant (Eq. (7)) also constrains, in the self-similar regime, the value of the turbulent dissipation rate defined as :

$$\overline{\varepsilon} = \nu \overline{\partial_j u_i \partial_j u_i} \, .$$

Indeed, knowing that the evolution of $\langle \overline{k} \rangle$ is $\partial_t(L\langle \overline{k} \rangle) = -L\langle \overline{\varepsilon} \rangle$, and that the differentiation of Eq. (7) implies that $\partial_t(L\langle \overline{k} \rangle) = -\mathrm{d}_t L(s_0+1)\langle \overline{k} \rangle$, one deduces that:

$$\overline{\omega}^G = \frac{\langle \overline{\varepsilon} \rangle}{\langle \overline{k} \rangle} = -(s_0+1)\frac{\mathrm{d}_t L}{L} \, . \tag{9}$$

Note that this relation is satisfied as soon as the regime is self-similar and Θ is given by Eq. (8).

Another consequence of the permanence of large eddies expressed by Eq. (6) concerns anisotropy. Indeed, large

eddies being permanent, they keep their initial anisotropy. Thus, even if the remaining scales of the spectrum return to isotropy, large scales will not. Therefore, the integral of the turbulent spectrum E_{ij} over $\boldsymbol{\kappa}$ will yield a Reynolds stress tensor which is anisotropic at all times. In [13], an estimate of this residual anisotropy was proposed for initial conditions representative of the passage of a shock on a linearly perturbed interface. This estimate allows to express as a function of s_0 the global anisotropy tensor b_{ij}^G. Within the framework proposed in [13], one has:

$$b_{33}^G \approx \frac{2}{3}\frac{s_0+3/2}{s_0+3+3(s_0+1)(s_0+2)a} \quad \text{with} \quad a \approx 0.3\,. \tag{10}$$

The smaller s_0 is, the larger the contribution of large scales is and the stronger the anisotropy is. The value of b_{33}^G varies approximately from $b_{33}^G = 0.1$ for $s_0 = 4$ to $b_{33}^G = 0.2$ for $s_0 = 0$.

The values of Θ and of b_{33}^G predicted in Eq. (8) and (10) are basic properties, characteristic of the self-similar state of Richtmyer–Meshkov turbulence. A statistical model, such as the generalized Langevin model, should be able to reproduce these properties.

3. The generalized Langevin model and its behavior in Richtmyer–Meshkov turbulence

The purpose of this section is to introduce the generalized Langevin model (GLM) and to show how this model behaves in Richtmyer–Meshkov turbulence. In particular, we would like to compare the predictions of the GLM against the expected properties of the self-similar states of Richtmyer–Meshkov turbulence described in Sec. 2 and more precisely to Eqs. (8) and (10).

3.1. Exact PDF equation and its modeling by a Langevin model

We introduce f the PDF of $\boldsymbol{u}$:

$$f(\mathbf{v}; x_3, t) = \overline{\delta(\mathbf{v} - \boldsymbol{u}(\boldsymbol{x}, t))}\,.$$

Its evolution equation is deduced from equation (1) using standard techniques [26, 36, 37]:

$$\begin{aligned}\partial_t f + \mathrm{v}_3\partial_3 f = \nu\partial_{jj} f - \partial_{\mathrm{v}_i}\left[\partial_3\overline{u_3^2}\delta_{i3} f - \overline{\left(\partial_i p'\middle|\mathbf{v}\right)} f\right] \\ -\partial^2_{\mathrm{v}_j\mathrm{v}_k}\left[\overline{\left(\varepsilon_{ik}\middle|\mathbf{v}\right)} f\right]\ ,\end{aligned} \tag{11}$$

where $\overline{\left(\cdot\middle|\mathbf{v}\right)}$ is the mean conditioned on $\mathbf{v}$ and where $\varepsilon_{ik} = \nu\partial_j u_i \partial_j u_k$. In this equation, the fluctuating acceleration $\overline{\left(\partial_i p'\middle|\mathbf{v}\right)}$ and the conditional dissipation $\overline{\left(\varepsilon_{ik}\middle|\mathbf{v}\right)}$ are not known explicitly in terms of the one point PDF f. These quantities involve two-point statistical information and need to be closed. One of the most popular model for closing $\overline{\left(\partial_i p'\middle|\mathbf{v}\right)}$ and $\overline{\left(\varepsilon_{ik}\middle|\mathbf{v}\right)}$ is the generalized Langevin model (GLM). This closure leads to the following modeled transport equation for f:

$$\partial_t f + \mathrm{v}_3\partial_3 f = -\partial_{\mathrm{v}_i}\left[\partial_3\overline{u_3^2}\delta_{i3} f + G_{ij}\mathrm{v}_j f\right] + \frac{C_0\overline{\varepsilon}}{2}\partial^2_{\mathrm{v}_j\mathrm{v}_j} f\ , \tag{12a}$$

with G_{ij} and C_0 model coefficients respecting the constraint:

$$\left(1 + \frac{3}{2}C_0\right)\overline{\varepsilon} + G_{ij}\overline{u_i u_j} = 0\,. \tag{12b}$$

Equation (12) must be supplemented by an evolution equation for the turbulent dissipation rate $\overline{\varepsilon}$. In this work, we will settle for the $\overline{\varepsilon}$ equation of a $\overline{k} - \overline{\varepsilon}$ model, with a turbulent transport term proportional to that of $\overline{k}$:

$$\partial_t\overline{\varepsilon} + \partial_3\left(C_\varepsilon\overline{\omega}\,\overline{u_3 k}\right) = -C_{\varepsilon_2}\overline{\omega}\,\overline{\varepsilon}\ , \tag{12c}$$

with C_ε and C_{ε_2} model constants, $\overline{u_3 k} = \frac{1}{2}\overline{u_3 u_i u_i}$ the advection flux of the kinetic energy and $\overline{\omega}$ the turbulent frequency, defined as:

$$\overline{\omega} = \frac{\overline{\varepsilon}}{\overline{k}}\,.$$

In the GLM setting, it is assumed that G_{ij} is a function of the anisotropy $\boldsymbol{b}$ and of whatever production term is involved. Since Richtmyer–Meshkov turbulence is devoid of any form of production, the tensor G_{ij} of the GLM can be expressed, in our particular case, as a function of anisotropy only:

$$G_{ij} = -\frac{1}{2}C_1\overline{\omega}\delta_{ij} + C_2\overline{\omega}\,b_{ij} + C_3\overline{\omega}\,b_{ij}^2\,.$$

Different values of C_1, C_2 and C_3 lead to different versions of the GLM. For instance, setting $C_1 = \mathrm{Cst}$ and $C_2 = C_3 = 0$ corresponds to the simplified Langevin model, and also, since there is no production to differentiate them, to the LRR-IP model. Setting $C_1 = (1 + \frac{3}{2}C_0) - 6C_2\overline{\omega}b_{ii}^3$, $C_0 = 2.1$, $C_2 = 3.5$, $C_3 = -3C_2$ yields the LIPM model. Other variants of the GLM can be found in [27, 28].

3.2. Corresponding evolution for the Reynolds stress tensor and its 0D reduction

By integrating Eq. (12) over $\mathbf{v}$ after multiplying it by $\mathrm{v}_i\mathrm{v}_j$, one obtains the evolution of the Reynolds stress tensor $\overline{R}_{ij}$ associated with the GLM.

$$\begin{aligned}\partial_t\overline{R}_{ij} + \partial_k\overline{u_k u_i u_j} = -\frac{2}{3}\overline{\varepsilon}\delta_{ij} \\ - 2\overline{\varepsilon}\left((C_1 - C_3 b_{kk}^2)b_{ij} - 2(C_2 + \frac{C_3}{3})\left(b_{ij}^2 - \frac{b_{kk}^2}{3}\delta_{ij}\right)\right)\,.\end{aligned} \tag{13}$$

In order to facilitate the analysis of this equation, we now assume that the dissipation $\overline{\varepsilon}$ and all the components of $\overline{u_i u_j}$ have similar spatial profiles. As a consequence, the

turbulent frequency $\overline{\omega}$ and b_{ij} are independent from space and depend only on time:

$$\text{0D assumption}: \ \overline{\omega} \equiv \overline{\omega}(t) \ , \ b_{ij} \equiv b_{ij}(t) = b_{ij}^G(t) \, .$$

Then, integrating the GLM equation for $\overline{R}_{ij}$ and that for $\overline{\varepsilon}$ (Eq. (12c)), we obtain that:.

$$\mathrm{d}_t\big(L\langle\overline{R}_{ij}\rangle\big) = -\frac{2}{3}\overline{\omega}L\langle\overline{k}\rangle\delta_{ij} - 2\overline{\omega}L\langle\overline{k}\rangle\Bigg[(C_1 - C_3 b_{kk}^2)b_{ij} - 2(C_2 + \frac{C_3}{3})\left(b_{ij}^2 - \frac{b_{kk}^2}{3}\delta_{ij}\right)\Bigg] \tag{14a}$$

$$\mathrm{d}_t\big(L\langle\overline{\varepsilon}\rangle\big) = -C_{\varepsilon_2}\overline{\omega}\, L\langle\overline{\varepsilon}\rangle \, . \tag{14b}$$

This system forms the 0D reduction of the GLM second order moment evolution. It offers insights into how the model behaves in the self-similar regime, as will be detailed in the next subsection. Note that the 0D reduction of turbulence models is a methodology that has already been extensively and successfully used to analyze Richtmyer–Meshkov and Rayleigh–Taylor turbulence. In particular, the 0D equations for the $\overline{k}$-$\overline{\varepsilon}$ model can be found in [38] and have proven useful in determining the properties of this model for turbulent mixing zones.

3.3. Self-similar solution to the 0D reduced model and main shortcomings of the GLM

The 0D reduction of the GLM admits a self-similar solution which is such that:

$$L \propto t^{\Theta} \ , \ \langle \boldsymbol{R} \rangle \propto t^{2\Theta-2} \quad \text{with} \quad \Theta = \frac{2C_{\varepsilon_2} - 3}{3C_{\varepsilon_2} - 3} \tag{15}$$

This self-similar solution is comparable to the one obtained from the theoretical predictions in Eq. (2). The value of the self-similar exponent Θ is however different: it depends on s_0 in the theoretical case (Eq. (8)) and on the constant C_{ε_2} in the GLM case. This difference is not *per se* a shortcoming of the GLM. Indeed, it can be resolved by simply setting the value of C_{ε_2} to reproduce the correct decay exponent of $\overline{k}$ and $\overline{\varepsilon}$, as will be discussed in the next section.

However, a stronger discrepancy arises in the way the GLM treats anisotropy. Indeed, from the 0D equations Eq. (14), one can show that the anisotropy tensor in the self-similar regime is solution to:

$$b_{33}^G\left(C_1 - 1 - (C_2 + C_3/3)b_{33}^G - \frac{3}{2}C_3(b_{33}^G)^2\right) = 0$$

This equation has at least one solution $b_{33}^G = 0$ and possibly multiple ones, depending on which model is considered. For instance, the LRR-IP and SLM have only the solution $b_{33}^G = 0$, while the LIPM has an additional one. When multiple solutions exist, b_{33}^G may go to one or another depending on initial conditions of $\langle\overline{k}\rangle$, $\langle\overline{\varepsilon}\rangle$ and b_{33}^G. Note that $b_{33}^G = 0$ corresponds to a full return to isotropy.

By contrast, Richtmyer–Meshkov turbulence exhibits a partial return to isotropy described by Eq. (10) depending on the initial infrared exponent s_0. The full return to isotropy predicted by some versions of the GLM (SLM,LRR-IP,...) is consequently not satisfactory. The additional anisotropic state predicted by other versions of the GLM is not sufficient either, even if it is parametrized to match the Richtmyer–Meshkov behavior. Indeed, depending on the initial conditions of the GLM, this additional solution may be reached or not. In the latter case, a full return to isotropy occurs again.

Therefore, one cannot reproduce satisfactorily the partial return to isotropy of Richtmyer–Meshkov turbulence with the existing versions of the GLM, where G_{ij} depends only on b_{ij}.

3.4. About the transport of turbulent kinetic energy

The evolution of $\overline{k}$ deduced from the Boussinesq equations (1) is:

$$\text{Exact evolution}: \ \partial_t\overline{k} + \partial_3\left(\overline{u_3 k} + \overline{u_3 p'} - \nu\partial_3\overline{k}\right) = -\overline{\varepsilon} \ , \tag{16}$$

with $\overline{\varepsilon} = \nu\overline{\partial_j u_k \partial_j u_k}$ the turbulent dissipation and $\overline{u_3 k} = \frac{1}{2}\overline{u_3 u_i u_i}$ the turbulent advection flux. Notwithstanding the viscous term, the evolution of $\overline{k}$ is governed by three physical processes: dissipation, turbulent advection and turbulent transport by the pressure flux. However, the GLM predicts another evolution. Taking the trace of Eq. (13) for $\overline{R}_{ij}$, one obtains that:

$$\text{GLM evolution}: \quad \partial_t\overline{k} + \partial_3\left(\overline{u_3 k}\right) = -\overline{\varepsilon} \, . \tag{17}$$

Comparing the evolution for $\overline{k}$ deduced from the GLM in Eq. (17) to its exact evolution in Eq. (16), we see that the GLM neglects the turbulent transport due to the pressure flux:

$$\overline{u_3 p'}\Big|^{\mathrm{GLM}} = 0 \, .$$

Discarding the pressure flux is relevant for particular situations [30], but there is no argument for doing so in Richtmyer–Meshkov turbulent flows. Hence, in its current formulation, it is likely that the GLM misses an important aspect of the evolution of the turbulent kinetic energy.

4. A Langevin model with partial return to isotropy

In the previous section, we identified two shortcomings of the GLM: its inability to reproduce correctly a partial return to isotropy and its absence of modeling for the turbulent pressure flux. In this section, we aim to address the first one of these shortcomings by introducing a two scale decomposition of the velocity field.

4.1. Two-scale decomposition of the velocity field

As explained in the introduction and in Sec. 2.3, the partial return to isotropy observed in Richtmyer–Meshkov turbulence is due to the permanence of large scales. The anisotropy of these scales remains constant throughout time and prevents the flow from becoming fully isotropic. In order to account for the behavior of large scales, we aim to isolate their contribution to the velocity field.

To this end, we consider the Fourier transform $\widehat{\boldsymbol{u}}(\boldsymbol{\kappa},t)$ of the velocity field taken at time t and wavevector $\boldsymbol{\kappa}$, as defined in Eq. (4) By definition, we can write the value of the velocity as:

$$u_i(\boldsymbol{x},t) = \int e^{\imath\boldsymbol{\kappa}\cdot\boldsymbol{x}}\widehat{u}_i(\boldsymbol{\kappa},t)\mathrm{d}\boldsymbol{\kappa}\,.$$

As a second step, we introduce a wave number κ_L which separates large permanent scales from smaller scales. We then split the definition of u_i into two contributions, a large and small scale one:

$$\begin{aligned} u_i &= u_i^L + u_i^S \qquad (18)\\ \text{with}\quad u_i^L &= \int_{\kappa\le\kappa_L} e^{\imath\boldsymbol{\kappa}\cdot\boldsymbol{x}}\widehat{u}_i(\boldsymbol{\kappa},t)\mathrm{d}\boldsymbol{\kappa}\\ \text{and}\quad u_i^S &= \int_{\kappa\ge\kappa_L} e^{\imath\boldsymbol{\kappa}\cdot\boldsymbol{x}}\widehat{u}_i(\boldsymbol{\kappa},t)\mathrm{d}\boldsymbol{\kappa}\,. \end{aligned}$$

4.2. Two-scale Langevin model

With this decomposition, we can now propose a simple adaption of the GLM accounting for the separate effects of large and small scales. In this respect, we note that the return to the mean term of the Langevin model, the one that controls the return to isotropy, can be written as:

$$G_{ij}\mathrm{v}_j = G_{ij}\overline{(u_j|\mathbf{v})} = G_{ij}\overline{(u_j^L|\mathbf{v})}f + G_{ij}\overline{(u_j^S|\mathbf{v})}\,.$$

The idea is then simply to differentiate the coefficients appearing before each of the conditional means. The model we propose takes the form:

$$\begin{aligned} &\partial_t f + \mathrm{v}_3\partial_3 f = \\ &\quad -\partial_{\mathrm{v}_i}\left[\partial_3\overline{u_3^2}\delta_{i3}f + G_{ij}^L\overline{(u_j^L|\mathbf{v})}f + G_{ij}^S\overline{(u_j^S|\mathbf{v})}f\right]\\ &\quad + \frac{C_0\overline{\varepsilon}}{2}\partial^2_{\mathrm{v}_j\mathrm{v}_j}f\ , \qquad (19a)\end{aligned}$$

with a condition similar to Eq. (12b):

$$\left(1+\frac{3}{2}C_0\right)\overline{\varepsilon} + G_{ij}^L\overline{u_iu_j^L} + G_{ij}^S\overline{u_iu_j^S} = 0\,. \qquad (19b)$$

Thus, with this formulation, we can control independently the return to isotropy of large and small scales while keeping the simple structure of the GLM.

Of course, this model is not yet closed: the conditional means $\overline{(u_j^L|\mathbf{v})}$ and $\overline{(u_j^S|\mathbf{v})}$ need to be precised, as well as the coefficients G_{ij}^L and G_{ij}^S.

4.3. Linear closure for the conditional means

The two conditional means $\overline{(u_i^L|\mathbf{v})}$ and $\overline{(u_i^S|\mathbf{v})}$ are related to one another through their definition (Eq. (18)), so that we only have to concentrate on one of them:

$$\overline{(u_i^L|\mathbf{v})} + \overline{(u_i^S|\mathbf{v})} = \mathrm{v}_i\,. \qquad (20)$$

Focusing on $\overline{(u_i^L|\mathbf{v})}$, we propose a linear closure of the form:

$$\overline{(u_i^L|\mathbf{v})} = M_{ij}^L\mathrm{v}_j\,. \qquad (21)$$

In order to estimate M_{ij}^L, we start from the exact definition of u_i^L (Eq. (18)) and derive that:

$$\begin{aligned} &\text{Exact relation}: \quad \langle\overline{u_iu_j^L}\rangle = \mathcal{R}_{ij}^L \qquad (22)\\ &\text{with}\quad \mathcal{R}_{ij}^L(t) = \frac{2\pi}{L}\int_{\kappa\le\kappa_L} E_{ij}(\boldsymbol{\kappa},t)\mathrm{d}\boldsymbol{\kappa}\,. \end{aligned}$$

Comparing this equation to the relation between spectrum and integrated Reynolds stresses (Eq. (5)), we see that $\langle\overline{u_iu_j^L}\rangle$ is the large scale contribution of $\langle\overline{R}_{ij}\rangle$. Besides, if we now use the linear model to express u_i^L, we also have:

$$\text{Modeled relation}: \quad \langle\overline{u_iu_j^L}\rangle = \langle M_{ik}^L\overline{R}_{kj}\rangle \qquad (23)$$

Comparing the modeled and exact expressions for $\langle\overline{u_iu_j^L}\rangle$ allows to set a constraint on M_{ij}^L. In order to fully exploit this constraint, we first propose an approximation for $\mathcal{R}_{ij}^L$. To do so, we write $\mathcal{R}_{ij}^L$ as:

$$\mathcal{R}_{ij}^L = 2\mathcal{K}^L\left(b_{ij}^L + \frac{1}{3}\delta_{ij}\right)\ ,$$

with $\mathcal{K}^L = \mathcal{R}_{pp}^L/2$ and b_{ij}^L the anisotropy tensor of $\mathcal{R}_{ij}^L$. Then, we assume that all the components of the initial spectrum $E_{ij}^{(0)}$ have the same infrared exponent s_0. As a result, b_{ij}^L is independent from time, with a value set by initial conditions. More precisely, for a mixing zone initiated by a shock crossing a linearly perturbed interface, one has, according to Ref. [13]:

$$b_{33}^L = \frac{2}{3}\frac{s_0+3/2}{s_0+3}\,. \qquad (24)$$

To estimate the large scale energy $\mathcal{K}^L$, we assume that the limit wave number κ_L separates a large scale range from a Kolmogorov inertial range, as proposed in [13]. Integrating this idealized spectrum, we obtain, as detailed in [13], that:

$$\mathcal{K}^L = \mathtt{x}^{\mathtt{L}}\langle\overline{k}\rangle \quad\text{with}\quad \mathtt{x}^{\mathtt{L}} = \frac{1}{1+3a\frac{(s_0+1)(s_0+2)}{(s_0+3)}}\ ,\ a\approx 0.3\,. \qquad (25)$$

Equating the two right-hand sides of Eqs. (22) and (23), with the proposed closure for $\mathcal{R}_{ij}^L$, we derive that:

$$\langle M_{ik}^L R_{kj}\rangle = \mathcal{R}_{ij}^L = 2\mathtt{x}^{\mathtt{L}}\langle\overline{k}\rangle\left(b_{ij}^L + \frac{1}{3}\delta_{ij}\right)\,.$$

This relation is verified in particular when:

$$M^L_{ik} R_{kj} = 2\mathtt{x}^{\mathtt{L}}\overline{k}\left(b^L_{ij} + \frac{1}{3}\delta_{ij}\right)$$

Multiplying this relation by the inverse of $\overline{R}_{kj}$, we deduce that:

$$M^L_{ij} = 2\mathtt{x}^{\mathtt{L}}\overline{k}\left(b^L_{ik} + \frac{1}{3}\delta_{ik}\right)\overline{R}^{-1}_{kj}\,. \tag{26}$$

Along with Eqs. (24) and (25), this expression provides a closure for M^L_{ij} and therefore for $\overline{(u^L_j|\mathbf{v})}$. This closure introduces an explicit dependency on the initial state of the flow, as required by the phenomenology of Richtmyer–Meshkov turbulence.

Note that through Eq. (20), the modeled expression for $\overline{(u^S_i|\mathbf{v})}$ is:

$$\begin{aligned}
&\overline{(u^S_i|\mathbf{v})} = M^S_{ij}\mathrm{v}_j \qquad (27)\\
\text{with}\quad &M^S_{ij} = \delta_{ij} - M^L_{ij} = 2\mathtt{x}^{\mathtt{S}}\overline{k}\left(b^S_{ik} + \frac{1}{3}\delta_{ik}\right)\overline{R}^{-1}_{kj}\\
\text{and}\quad &\mathtt{x}^{\mathtt{S}} = 1 - \mathtt{x}^{\mathtt{L}} = \frac{3a(s_0+1)(s_0+2)}{s_0+3+3a(s_0+1)(s_0+2)}\\
&b^S_{ij} = \frac{b_{ij} - \mathtt{x}^{\mathtt{L}} b^L_{ij}}{1-\mathtt{x}^{\mathtt{L}}}\,.
\end{aligned}$$

4.4. Model coefficients

As a last step in the derivation of our model, we need to precise the values of G^L_{ij} and G^S_{ij}. The value of G^L_{ij} is tied to the evolution of large scales and should yield a correct evolution for $\mathcal{R}^L_{ij}$ when $\mathtt{x}^{\mathtt{L}} = 1$. The exact evolution can be deduced using the principle of permanence of large scales. Indeed, given its definition (Eq. (22)), $\mathcal{R}^L_{ij}$ involves only scales which are permanent. It can be rewritten using the initial spectrum

$$\mathcal{R}^L_{ij}(t) = \frac{2\pi}{L}\int_{\kappa\le\kappa_L} E^{(0)}_{ij}(\boldsymbol{\kappa})\mathrm{d}\boldsymbol{\kappa}.$$

Then, differentiating this equation with respect to time, knowing that $E^{(0)}_{ij}(\boldsymbol{\kappa}) \propto \kappa^{s_0-2}$ and assuming self-similarity so that $\kappa_L \propto 1/L$, we deduce that:

$$\partial_t\Big(L\mathcal{R}^L_{ij}\Big) = -(s_0+1)\ \mathrm{d}_t L\ \mathcal{R}^L_{ij}\,.$$

Finally, knowing the relation between $\overline{\omega}^G$ and $\mathrm{d}_t L$ given in Eq. (9), we deduce that:

$$\text{For permanent eddies :}\quad \partial_t\Big(L\mathcal{R}^L_{ij}\Big) = -L\overline{\omega}^G\mathcal{R}^L_{ij}\,. \tag{28}$$

This equation is valid for $\mathcal{R}^L_{ij}$ whatever the value of $\mathtt{x}^{\mathtt{L}}$. Now, when $\mathtt{x}^{\mathtt{L}} = 1$, one also has by definition $\langle\overline{R}_{ij}\rangle = \mathcal{R}^L_{ij}$. As a result, in that particular case, one can also compute the modeled evolution of $\mathcal{R}^L_{ij}$ by multiplying the PDF equation (19) by $\mathrm{v}_i\mathrm{v}_j$ and by integrating it over $\mathbf{v}$ and x_3. Taking into account that $\overline{(u^S_i|\mathbf{v})} = 0$ and identifying $\langle\overline{R}_{ij}\rangle$ and $\mathcal{R}^L_{ij}$, this procedure yields :

$$\begin{aligned}
&\text{PDF model for } \mathtt{x}^{\mathtt{L}} = 1 :\\
\partial_t\Big(L\mathcal{R}^L_{ij}\Big) &= L\left(G^L_{ik}\mathcal{R}^L_{kj} + G^L_{jk}\mathcal{R}^L_{ki}\right)\\
&-\frac{2}{3}L\left(\overline{\omega}^G\mathcal{K}^L + G^L_{kl}\mathcal{R}^L_{kl}\right)\delta_{ij}
\end{aligned} \tag{29}$$

For equations (28) and (29) to be equivalent, G^L_{ij} must verify:

$$G^L_{ij} = -\frac{1}{2}C^L_1\overline{\omega}\delta_{ij} \quad\text{with}\quad C^L_1 = 1\,.$$

As for G^S_{ij}, we note that the closures used in the standard GLM are usually proposed for describing processes occurring at small inertial scales. Therefore, we propose to use the same closures as those used for standard GLM to set G^S_{ij}. More precisely, we will use the simplified Langevin model. At this point, there is indeed no reason to look for more complex closures. We thus set :

$$G^S_{ij} = -\frac{1}{2}C^S_1\overline{\omega}\delta_{ij}\ \ ,$$

In the literature, the value of C^S_1 varies widely in the literature, from $C_0 \approx 1.8$ to $C^S_1 \approx 10$ [39]. The highest values are usually obtained when connecting C^S_1 to the Kolmogorov constant defining the Lagrangian two-time spectrum in the inertial range. On the other hand, the lowest values are obtained by identification of C^S_1 to the return to isotropy constant appearing in several RSM, such as the LRR model [40]. In this work, we are not interested in predicting the two-time statistics of homogeneous isotropic turbulence. We would rather obtain a correct prediction of the return to isotropy of the Reynolds stresses. Thus, we will use a value of C^S_1 coming from a RSM model called GSG [41] and which has been thoroughly validated against experiments and simulations for Richtmyer–Meshkov and Rayleigh–Taylor turbulence. In agreement with this model, we will set:

$$C^S_1 = 1.8\,.$$

Note that the value of C_0 is related to C^S_1 by Eq. (19b). With the prescribed expressions of G^S_{ij} and G^L_{ij}, we derive from this relation that:

$$C_0 = \frac{2}{3}\mathtt{x}^{\mathtt{S}}(C^S_1 - 1)\,. \tag{30}$$

In addition to G^S_{ij} and G^L_{ij}, we must also specify the coefficients for the $\overline{\varepsilon}$ equation. Note that this equation is not modified and remains given by Eq. (12c). In this equation, we set C_ε to 1, assuming that the transport of $\overline{\varepsilon}$ is on par with that of $\overline{k}$. As for C_{ε_2}, we aim ensure that the correct growth rate exponent of the mixing zone is obtained. Thus, we set the value of C_{ε_2} so that Eqs. (15) and (8) agree. This yields:

$$C_{\varepsilon_2} = \frac{1-\Theta}{\frac{2}{3}-\Theta} = \frac{3}{2}\frac{s_0+2}{s_0+1}\,. \tag{31}$$

Note that this expression was first derived in [12].

4.5. Final expression of the model and its 0D reduction

With these different specifications, the modified two-scale GLM can be written as:

$$\begin{aligned}\partial_t f + \mathrm{v}_3\partial_3 f = \\ - \partial_{\mathrm{v}_i}\left[\partial_3\overline{u_3^2}\delta_{i3}f - \frac{1}{2}\overline{\omega}\left(C_1^L M_{ij}^L + C_1^S M_{ij}^S\right)\mathrm{v}_j f\right] \\ + \frac{C_0\overline{\varepsilon}}{2}\partial^2_{\mathrm{v}_j\mathrm{v}_j} f \ ,\end{aligned} \tag{32}$$

with $C_1^L = 1$, $C_1^S = 1.8$, C_0 given by Eq. (30), M_{ij}^L given by Eq. (26) and M_{ij}^S given by Eq. (27). The value of $\overline{\varepsilon}$ is obtained from Eq. (12c) with $C_\varepsilon = 1$ and C_{ε_2} given by Eq. (31).

In order to compare this modified two-scale model with the original GLM formulation, we integrate Eq. (32) over $\mathbf{v}$ after multiplying it by $\mathrm{v}_i\mathrm{v}_j$. We thus obtain the evolution of the Reynolds stress tensor $\overline{R}_{ij}$ associated with the modified GLM:

$$\begin{aligned}\partial_t\overline{R}_{ij} + \partial_k\overline{u_k u_i u_j} = -2\overline{\varepsilon}\Big(C_1^S b_{ij} - (C_1^S - 1)\mathtt{x}^{\mathtt{L}} b_{ij}^L\Big) \\ -\frac{2}{3}\overline{\varepsilon}\delta_{ij}\,.\end{aligned} \tag{33}$$

Compared to Eq. (13), we see that, instead of letting b_{33} tend to 0, the modified GLM lets b_{33} relax toward a value which is set by initial conditions at large scales. This aspect is better illustrated when looking at the 0D reduced equation of the proposed model. With the same assumptions as the one we used to derive Eqs. (14) for the initial model, we obtain that:

$$\mathrm{d}_t b_{ij}^G = -(C^S - 1)\overline{\omega}^G\left(b_{ij}^G - \mathtt{x}^{\mathtt{L}} b_{ij}^L\right)\,.$$

Thus, instead of letting b_{ij}^G tend to 0, the modified GLM predicts that it tends to $\mathtt{x}^{\mathtt{L}} b_{ij}^L$. One can verify that $\mathtt{x}^{\mathtt{L}} b_{33}^L = \frac{2}{3}\frac{s_0+3/2}{s_0+3+3(s_0+1)(s_0+2)a}$, which is the desired value predicted in [13]. The modified GLM consequently meets its assigned objective of correctly predicting the anisotropy of a Richtmyer–Meshkov mixing zone. As for the growth rate of the mixing zone, the formula (15) still apply to the modified GLM. Hence, with C_{ε_2} specified by Eq. (31), the modified GLM predicts the correct value of Θ.

5. Transport by the pressure flux

The second weakness of the GLM we identified concerned the fact that it does not account for the effects of the velocity pressure correlation $\overline{u_i'p'}$ on the transport of kinetic energy. More precisely, among the different variants of the GLM which have been proposed in the literature, only Ref. [29] proposes a closure for this term. But even this closure is not entirely satisfying since it is not conservative.

By contrast, $\overline{u_i'p'}$ is taken into account in other types of models and in particular in Reynolds stress models (RSM) which are deeply connected to PDF closures [28]. Therefore, the idea we pursue in this section is the following. First, we aim to identify how $\overline{u_i'p'}$ is dealt with in RSM formulations. Then, we propose a simple method for integrating some existing RSM closures of $\overline{u_i'p'}$ into the Langevin PDF model (32).

5.1. On transport by the pressure flux in RSM

In the evolution of the Reynolds stress tensor, turbulent transport arises from the velocity/pressure gradient correlation:

$$\Pi_{ij} = -\left[\overline{u_i\partial_j p'} + \overline{u_j\partial_i p'}\right]\,.$$

This correlation can be split into a pressure flux term T_{ij}^p and a trace-free redistribution term ϕ_{ij} representing inter-component energy transfer:

$$\Pi_{ij} = T_{ij}^p + \phi_{ij} \quad \text{with} \quad \phi_{ii} = 0 \quad \text{and} \quad T_{ii}^p = \partial_i\overline{u_i p'}\,.$$

As noted by [42] and [43], this decomposition is not unique. The most frequently used decomposition is

$$\phi_{ij} = \overline{p'\left(\partial_j u_i + \partial_i u_j\right)} \ \text{and} \ T_{ij}^p = -\partial_k\left(\overline{u_i p'}\delta_{jk} + \overline{u_j p'}\delta_{ik}\right)\,. \tag{34a}$$

Another one proposed in [42] is:

$$\phi_{ij}^* = \left[\Pi_{ij} + \frac{2}{3}\partial_k\overline{u_k p'}\,\delta_{ij}\right] \quad \text{and} \quad T_{ij}^{p*} = -\frac{2}{3}\partial_k\overline{u_k p'}\,\delta_{ij}\,. \tag{34b}$$

Finally, in Ref. [43], the following was suggested:

$$\phi_{ij}^\dagger = \left[\Pi_{ij} + \frac{R_{ij}}{\overline{k}}\partial_k\overline{u_k p'}\right] \quad \text{and} \quad T_{ij}^{p\dagger} = -\frac{R_{ij}}{\overline{k}}\partial_k\overline{u_k p'} \tag{34c}$$

In homogeneous turbulence, all decompositions are equivalent: the pressure flux term vanishes and one is left with $\Pi_{ij} = \phi_{ij} = \phi_{ij}^* = \phi_{ij}^\dagger$. This equivalence leads to an important issue. Indeed, all closures for Π_{ij} are derived for the case of homogeneous turbulence and can equally be viewed as closures for ϕ_{ij}, ϕ_{ij}^* or $\phi_{ij}^\dagger$. For inhomogeneous flows, this ambiguity has to be solved. However, there is no clear theoretical argument that would allow to discriminate which of ϕ_{ij}, ϕ_{ij}^* or $\phi_{ij}^\dagger$ is closed. Some lines of argument have been proposed by [44], [45] or [46], each favoring one of the three different possible interpretations. But they are somewhat subjective and cannot be received as definitive.

Given this confusion, we adopt a pragmatic point of view. Among the three listed decomposition, only the one proposed by [43] can be easily translated in terms of a GLM model. [29] already noted the difficulty in using the first decomposition in GLM. Similar arguments also apply to the second decomposition. We note that the decomposition of [43] is also the one retained by [47] and [48], also for practical reasons.

5.2. Expression of the PDF model for transport by the pressure flux

With the decomposition (34c), it is easy to adapt the GLM in its original or modified form (Eqs. (12) and (32)). Indeed, we only need to add a term to the GLM so that its corresponding Reynolds stress evolution accounts for the presence of $T_{ij}^{p\dagger}$. Starting from Eq. (32), this can be done in the following way:

$$\begin{aligned}\partial_t f + \mathrm{v}_3\partial_3 f = \\ -\partial_{\mathrm{v}_i}\left[\partial_3\overline{u_3^2}\delta_{i3}f - \frac{1}{2}\overline{\omega}\left(C_1^L M_{ij}^L + C_1^S M_{ij}^S\right)\mathrm{v}_j f - \frac{\Omega_P}{2}\mathrm{v}_i\right] \\ + \frac{C_0\overline{\varepsilon}}{2}\partial^2_{\mathrm{v}_j\mathrm{v}_j} f \ , \\ \text{with} \quad \Omega_P = \frac{1}{\overline{k}}\partial_k\overline{u_k p'}\,.\end{aligned} \tag{35}$$

The additional term is the one proportional to the frequency Ω_P. The value of Ω_P depends on the gradient of $\overline{u_k p'}$ and can be positive or negative. In order to evaluate this frequency, we must provide a closure for $\overline{u_k p'}$

In the RSM approaches, several closures have been proposed for $\overline{u_k p'}$ [30, 47, 49, 50]. Most of these closures differ in the way they treat the rapid part of the pressure field, i.e. the part generated by mean flow distortions. In Richtmyer–Meshkov turbulence, there is no distortion and most of these models revert to the one originally proposed by Lumley [49], namely:

$$\text{Lumley}: \ \overline{u_i p'} = -\frac{2}{5}\overline{u_i k} \tag{36}$$

While not shown here, this formula turns out to be an accurate prediction for the pressure flux in Richtmyer–Meshkov turbulence.

6. Validation

In order to validate the two-scale Langevin model derived in the previous sections, we compare it against several large eddy simulations (LES) of Richtmyer–Meshkov turbulent mixing zones. The Langevin model itself (Eq. (35) is solved numerically using a Lagrangian Monte Carlo (LMC) method. The LES, LMC simulations and their comparisons are detailed in the remaining of this section.

6.1. Description of the large eddy simulations

For our validation purposes, we consider the same LES of Richtmyer–Meshkov turbulence as those used in Ref. [13]. For the sake of completeness, the details of these simulations are repeated hereafter. First of all, these LES are implicit (ILES) and are performed with the code TRICLADE, a massively parallel code intended to solve turbulent mixing of perfect gases in a variable density context [51]. A shock capturing scheme provides just enough numerical viscosity and diffusivity to ensure stability. More precisely, for this work, we use a conservative finite difference scheme based on the wave propagation algorithm of LeVeque [52], with high accuracy provided by the corrections due to Daru and Tenaud [53]. Directional splitting is used, and uniform time–space accuracy for one-dimensional problems is reached thanks to the kind of Cauchy–Kovalevsky procedure of [53]. Time–space accuracy of fifth-order is used here, and a monotonicity preserving limitation is applied, as described by [53].

Table 1 summarizes the main parameters of the simulations. The domain is of size $L_{\mathrm{dom}} \times L_{\mathrm{dom}} \times 1.5L_{\mathrm{dom}}$ and is discretized by a regular grid with $N \times N \times 1.5N$ cells. The Atwood is chosen small and the shock Mach number is set to $M_S = 2.8$.

Atwood number	$\mathtt{A}_t = 0.05$
Shock Mach number	$M_S = 2.8$
Grid resolution	$N = 1024$
Domain size	$L_{\mathrm{dom}} = 1$

Table 1: Main simulation parameters

In [11], comparisons were made between two types of initialization. The first one consists in looking at the evolution of a Richtmyer–Meshkov turbulent mixing zone by simulating a shock crossing a perturbed interface. In the second one, the shock is not accounted for. Instead, the simulation is directly initialized by injecting at the perturbed interface a vorticity field stemming from the linear analysis of the Richtmyer–Meshkov instability. The differences between the two types of initialization were found to be negligible. Therefore, in this work, we opt for the second type of initialization. Indeed, it greatly alleviates the computational cost of the simulation, as the shock structure does not need to be solved explicitly and as the domain length can be reduced in the inhomogeneous direction.

Thus, at initial time, the simulation is set by imposing a perturbed interface and a perturbed vorticity field at the center of the domain. The perturbed interface is defined by its power spectrum P_h which is set to:

$$P_h(k_\perp) = \overline{h^2}k_0^{-1}\,\frac{2^{(s_0+2)/2}}{\Gamma(\frac{s_0}{2})}\,\left(\frac{k_\perp}{k_0}\right)^{s_0-1} e^{-2(k_\perp/k_0)^2} \ ,$$

where $s_0 - 1$ is the exponent of P_h at large scales, k_0 is a cut-off wavenumber at small scales and $\overline{h^2}$ is the variance of the perturbation interface. The velocity field induced by the linear Richtmyer–Meshkov instability is imposed according to the description given in [13]. The same procedure as the one prescribed in App. B of Ref. [11] is used.

In all the simulations performed hereafter, the cut-off wavenumber k_0 and the perturbation height variance are chosen equal to:

$$k_0 = \frac{2\pi}{\lambda_0} = \frac{\pi}{4\Delta x} \ \text{ and } \ \frac{\sqrt{\overline{h^2}}}{\Delta x} = 2.5 \quad \text{with} \quad \Delta x = \frac{L_{\mathrm{dom}}}{N}.$$

The infrared exponent s_0 is varied from 0 to 4. More precisely, 5 simulations are performed with the following values of s_0:

$$\text{values of } s_0: \quad 0 \ , \ 1 \ , \ 2 \ , \ 3 \ , \ 4$$

The different simulations we perform unfold similarly. After a short transient, including a linear phase, the simulations approach a state where the length of the mixing zone $L(t)$ and the different one point second-order correlations of velocity and concentration obey approximate power laws. This evolution is indicative of a self-similar regime and is reached at approximately the same non-dimensional time for all simulations, i.e. for $t \geq t_0$ with:

$$t_0 \approx 3t_{ref} \quad \text{with} \quad t_{ref} = \frac{\lambda_0^2}{\sqrt{\overline{h^2}}\mathtt{A}_t \Delta U} \, .$$

Details about this evolution can be found in Ref. [13].

6.2. Description of the PDF model simulations

The same configuration as the one described in the previous section is also simulated using the two-scale Langevin PDF model proposed in this work. To this end, we use a Lagrangian Monte Carlo (LMC) method to solve Eq. (35). This method is second order accurate in time and space and is fully described in [54]. The LMC simulations reported hereafter are performed by following the stochastic evolutions of $N_p = 10^5$ Lagrangian particles per cells, on a grid of $N_x = 512$ cells discretizing the same domain as the LES.

The LMC simulations are initialized at $t \approx t_0$, i.e. when the flow becomes self-similar. At this time, we extract, from the LES, planes perpendicular to $\boldsymbol{x}_3$ and located at the positions of the Monte Carlo grid cell centers. Then, we attribute to each Lagrangian particle in a given cell a velocity field sampled from the 1024×1024 points of the corresponding extracted plane. This ensures that the one point PDF of the velocity field at initial time converges towards the PDF of the LES simulation when N_p increases.

Besides, to initialize the LMC simulations, we must also specify a value for the mean dissipation $\overline{\varepsilon}$. Since we are using implicit LES, we do not have access to an explicit value of this quantity. Still, we can determine the overall integrated value of the dissipation. Indeed, from Eq. (16), we have:

$$\partial_t \int \overline{k} \mathrm{d}x_3 = - \int \overline{\varepsilon} \mathrm{d}x_3 \, .$$

Knowing the time evolution of $\int \overline{k} \mathrm{d}x_3$, we can compute its derivative and estimate $\int \overline{\varepsilon} \mathrm{d}x_3$. To obtain a local value of $\overline{\varepsilon}$, we then assume that $\overline{\varepsilon}$ and $\overline{k}$ share the same spatial profile. With this hypothesis, we can initialize $\overline{\varepsilon}$ as follows:

$$\text{At } t = t_0 \ , \ \overline{\varepsilon}(x_3) = \frac{\int \overline{\varepsilon} \mathrm{d}x_3}{\int \overline{k} \mathrm{d}x_3} \overline{k}(x_3) \, .$$

This completes the initialization procedure of the LMC simulations.

6.3. Self-similar evolution

The two-scale Langevin PDF model Eq. (35) was designed with the explicit purpose of reproducing the self-similar evolutions of the mixing zone with, the kinetic energy and the anisotropy of the Reynolds stresses in Richtmyer–Meshkov turbulence. To check whether the first of these purposes is met, we introduce the half-width of the mixing zone:

$$\begin{aligned} & L_k = x^+_{1/2} - x^-_{1/2} \\ \text{with} \quad & x^\pm_{1/2} \quad \text{such that} \quad \overline{k}(x^\pm_{1/2}) = \max \overline{k} \\ \text{and} \quad & x^+_{1/2} > 0 \ , \ x^-_{1/2} < 0 \, . \end{aligned}$$

Figure 2 shows the evolution of L_k for different values of s_0. It can be seen that the two-scale Langevin PDF model yields an evolution of L_k which is close to the one obtained from the LES. The largest differences are observed for the case $s_0 = 1$. Both LES and Langevin model evolutions remain close to the predicted power law $L_k \propto t^\Theta$ with $\Theta = 2/(s_0 + 4)$.

Similar observations are made for the decay of the kinetic energy, as given by the evolution of $\max(\overline{k})$. The two-scale Langevin model follows closely the LES simulations and both evolve approximately as the expected power law $\max(\overline{k}) \propto t^{-2(1-\Theta)}$.

Finally, larger differences are seen for the global anisotropy b^G_{33} as defined by Eq. (3), especially for $s_0 = 1$. Still, the two-scale Langevin model retrieves the correct trend of increasing anisotropy with decreasing s_0 and yields value which are globally on par with the LES simulation.

In order to obtain a more synthetic comparison of the self-similar properties discussed above, we measure the growth exponent Θ by doing a least-square fit of a power law on the evolution of L_k, from $t \geq t_0$. The value of the fitted power law exponent is displayed for the LES and the two-scale Langevin model in Fig. 5a as a function of s_0. It is also compared against the theoretical prediction Eq. (8). A good agreement is observed between the different simulation results and the predicted value. Note that the LES points shown in Fig. 5a are different from those displayed in [13]. Indeed, the definition of Θ used in [13] is based on the mean concentration profile and not on the kinetic energy. Similarly, Fig. 5b shows the value of b^G_{33} at the end of the simulations for the LES and Langevin model. It can be seen that the two-scale Langevin model reproduces the variations of anisotropy as a function of s_0.

In addition, Fig. 5a and 5b display results obtained from simulations done with the standard simplified Langevin model (SLM). We recall that this model is given by Eq. (12) with $G_{ij} = -C_1 \overline{\omega} \delta_{ij}$, or equivalently by setting $C_1^L = 0$, $M^S_{ij} = \delta_{ij}$ and $\Omega_P = 0$ in the two-scale equation (35). The value of the SLM constants are set to $C_1 = 4.15$ and $C_{\varepsilon_2} = 1.92$, which are two of the most frequently used values for these coefficients. The drawbacks of the SLM mentioned in the introduction can be clearly observed in

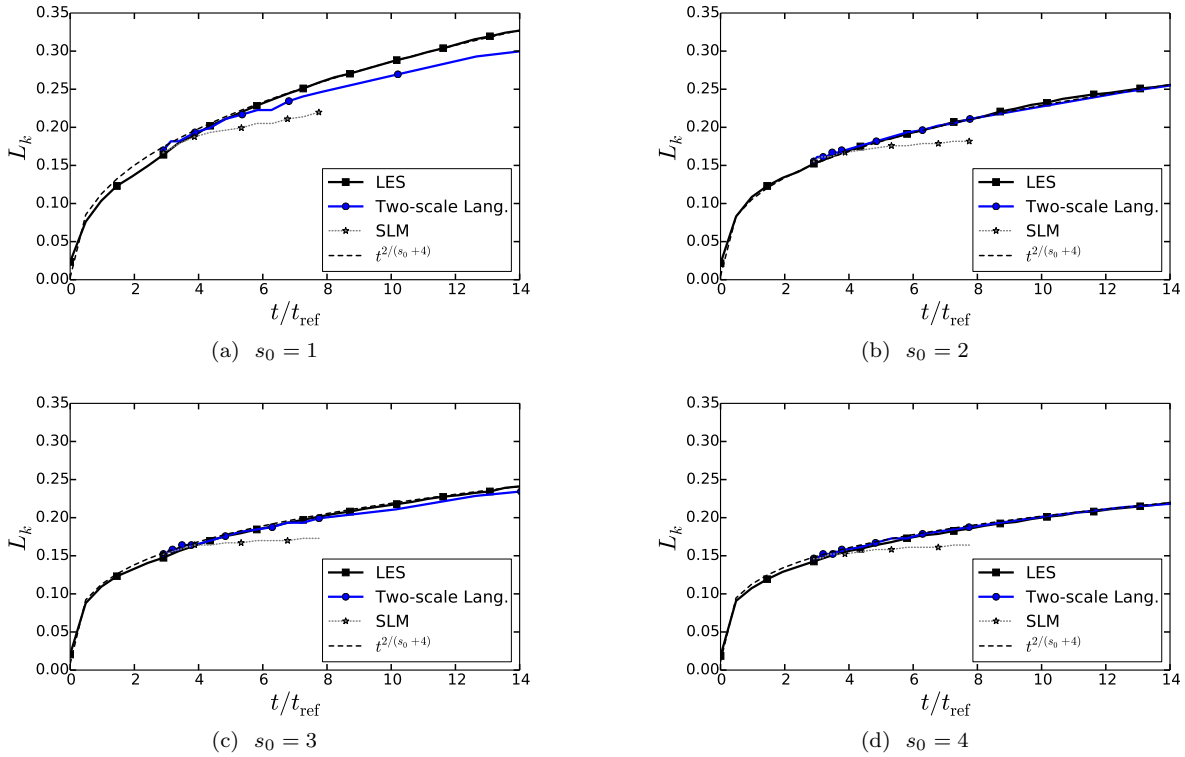

(a) $s_0 = 1$ (b) $s_0 = 2$

(c) $s_0 = 3$ (d) $s_0 = 4$

Figure 2: Evolution of L_k

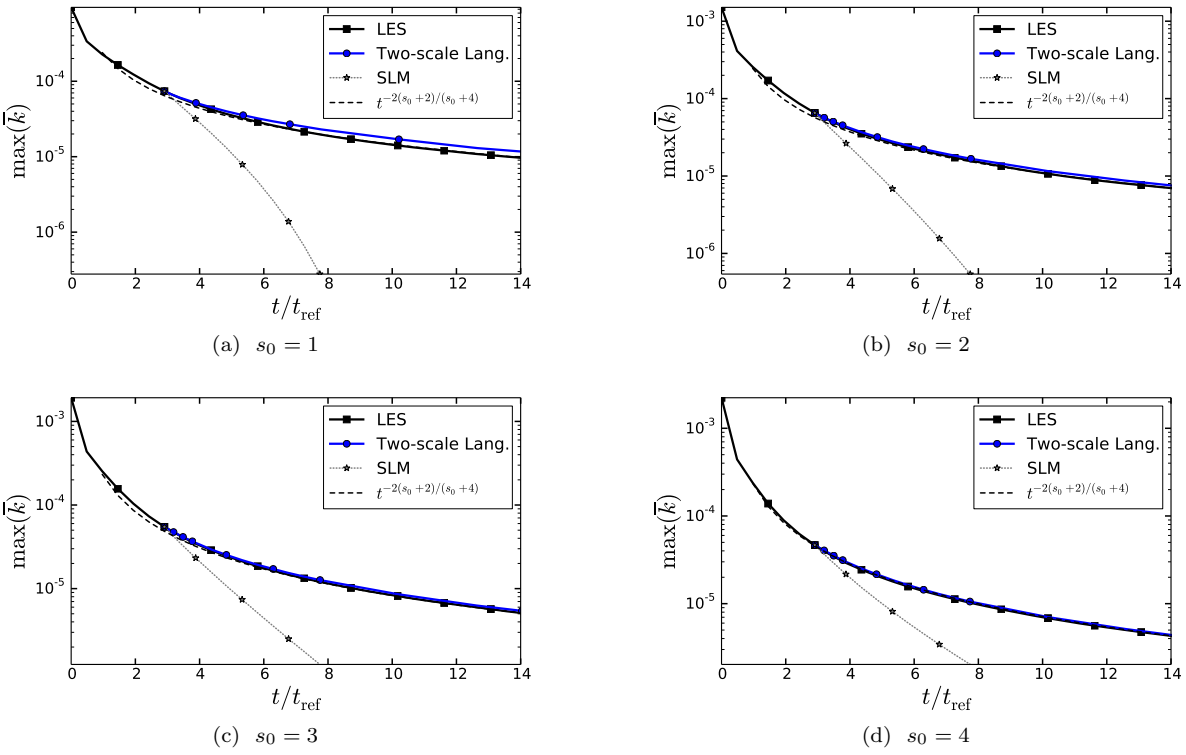

(a) $s_0 = 1$ (b) $s_0 = 2$

(c) $s_0 = 3$ (d) $s_0 = 4$

Figure 3: Evolution of $\max(\bar{k})$

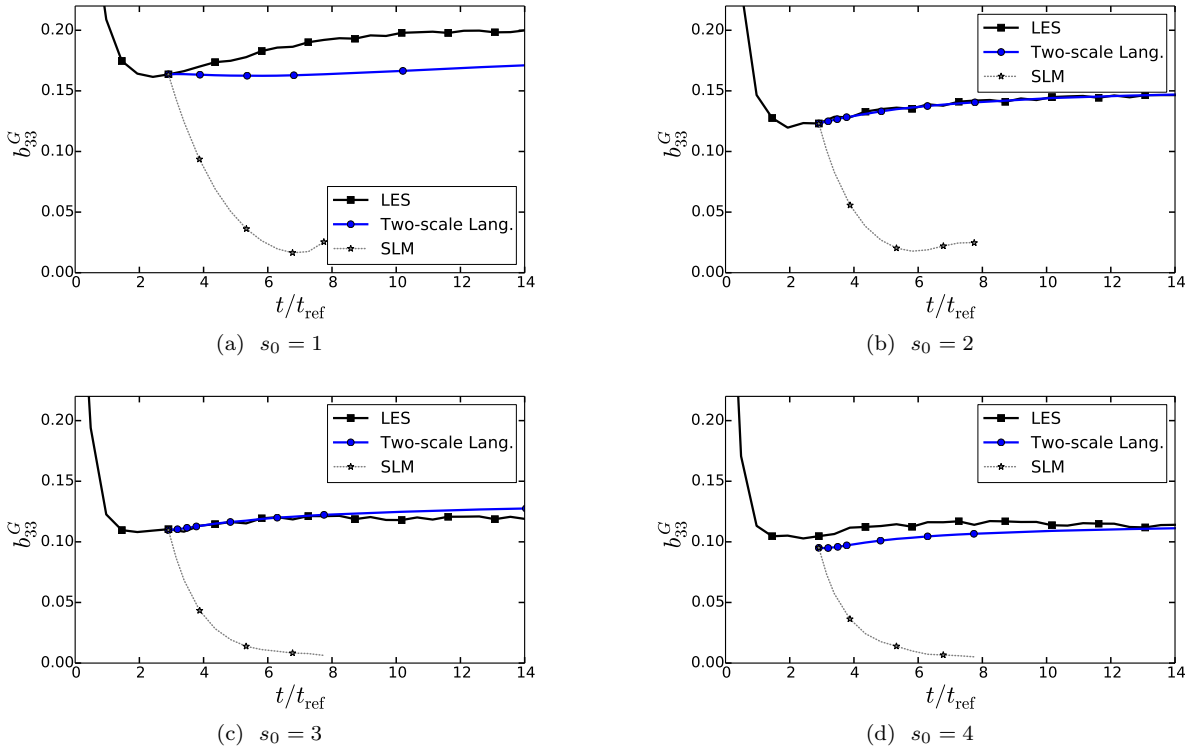

(a) $s_0 = 1$ (b) $s_0 = 2$

(c) $s_0 = 3$ (d) $s_0 = 4$

Figure 4: Evolution of $\max(\overline{k})$

these figures. It can be seen that the growth exponent Θ does not match the expected one and that a strong, almost complete, return to anisotropy occurs. The proposed two-scale Langevin model improves those two aspects.

6.4. Role of the pressure flux term

Another focus of the present work is the role played by turbulent transport by the pressure flux. To account for this effect, we added in our model (Eq. (35)) a term proportional to the pressure frequency $\Omega_P = \partial_k \overline{u_k p'}/\overline{k}$. The effect of this additional term is assessed hereafter by comparing two sets of LMC simulations. The first one is done by including the pressure term and the second one by discarding it, i.e. by setting $\Omega_P = 0$.

The main observation is that the mixing zone width obtained without accounting for the pressure term is systematically larger than the one obtained with it. Besides, while the width predicted by the full model remains close to the LES results, this is not the case anymore when $\Omega_P = 0$. These aspects are illustrated in Fig. 6a for the simulation with $s_0 = 2$. The origin of this property can be traced back to the differences in the kinetic energy flux of the two models. When Ω_P is accounted for, the flux is equal to $\overline{u_3 k} + \overline{u_3 p'} \approx \frac{3}{5}\overline{u_3 k}$ while it is equal to $\overline{u_3 k}$ otherwise. Since $\overline{u_3 k}$ is initially the same for the two simulations, the energy flux is higher for the case with $\Omega_P = 0$ and the mixing zone width increases faster, at least initially. Accordingly, the decrease of the maximum kinetic energy is also faster.

Another systematic effect concerns anisotropy. In Fig. 6b, one can see that the model with $\Omega_P = 0$ slightly over-predicts b_{33}^G compared with the full model. This result is shown for the simulation with $s_0 = 2$ but it applies equally well to the other ones. This difference can be attributed to the fact that the Ω_P term is akin to an additional return to isotropy term. Hence its presence leads to a decrease in anisotropy.

As a whole, accounting for the pressure term appears fundamental for ensuring the coherence between the LES and the Langevin model results. Without it, differences on the order of 10% are observed on the mixing zone width and maximum kinetic energy.

6.5. Spatial profiles

The two-scale Langevin model has been designed to reproduce the $0D$ self-similar evolutions of the mixing zone width, kinetic energy and anisotropy. As shown in the previous subsections, the model is indeed successful in performing this task. The question we would like to examine here is whether the model can also predict correct spatial profiles and not only some of their integrals. Fig. 7 displays the spatial profiles of $\overline{u_3'^2}$ and $\overline{u_1'^2}$ at the end of the simulation with $s_0 = 2$. It can be seen that the two-scale Langevin model yields spatial profiles which are in good agreement with the LES. In particular, the model predicts spatial profiles which are not parabolic, as would

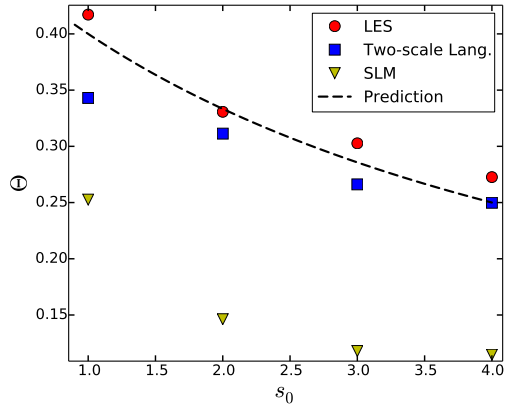

(a)

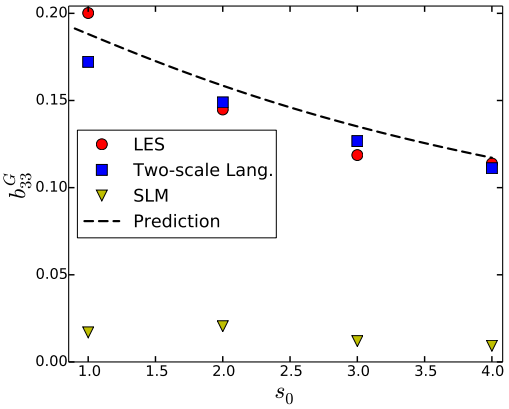

(b)

Figure 5: Θ and b_{33}^G at the end of the simulations, as a function of s_0

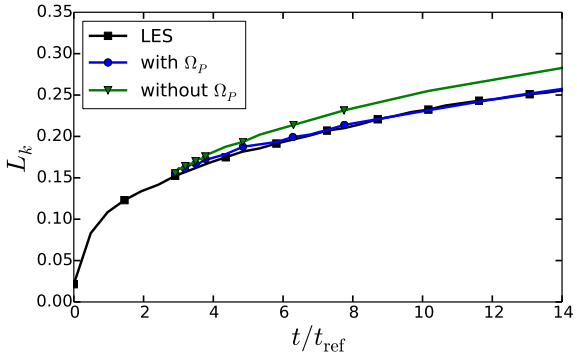

(a)

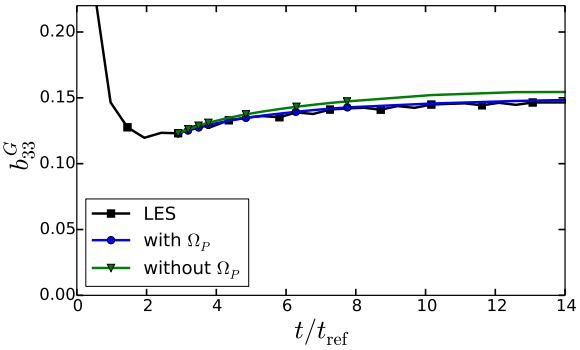

(b)

Figure 6: Influence of the transport by the pressure flux on the evolution of L_k and b_{33}^G for the simulation with $s_0 = 2$.

RSM do, but are thinner at the center and display tails on the edges. Similar comparisons also apply to the other simulations with different s_0.

6.6. PDF of the longitudinal velocity

To conclude the validation of the two-scale Langevin model, we investigate the shapes of the PDF of the longitudinal velocity u_3. Overall, a good agreement is observed between the LES and the two-scale Langevin model, as shown in Figs. 8-11. In particular, the emergence of a peak at negative velocities, its position and amplitude, is correctly reproduced by the model. This feature of the PDF has been analyzed in [55]. It is attributed to the effects of inhomogeneity and more specifically to the gradient of kinetic energy.

What is more, the model also correctly captures the dependency of the PDF shape on initial conditions. This dependency is most evident close to the center of the mixing zone. For $s_0 = 4$, the PDF at $x_3/L_k \approx 0$ is close to a Gaussian. As s_0 decreases, the shape of the PDF becomes squarer (see Fig. 8) until two small peaks arise close to $v_3 = 0$, for $s_0 = 1$. At other positions, the PDF becomes more asymmetric as s_0 decreases from 4 to 1.

Beyond the sole validation of the two-scale Langevin model, we would like to point out that the evolution of the PDF with s_0 is, in itself, a striking result. Indeed, the permanence of large-eddies predicts a dependency on initial conditions for second-order correlations but does not say anything about higher order correlations. Figures 8-11 show that this dependency extends to the whole PDF and its associated one-point statistics.

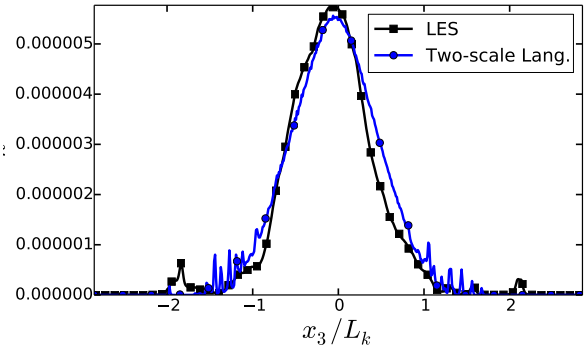

(a) $\overline{u_3'^2}$

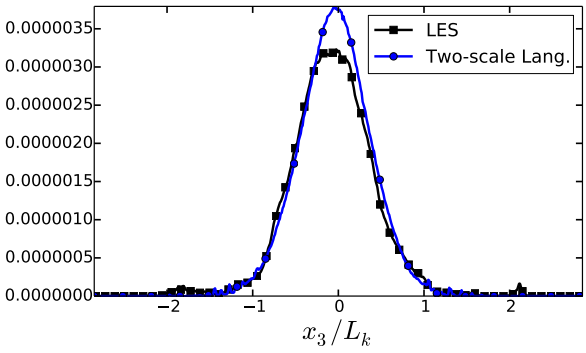

(b) $\overline{u_1'^2}$

Figure 7: Influence of the transport by the pressure flux term on the evolution of L_k and b_{33}^G for the simulation with $s_0 = 2$.

7. Conclusion

Despite their apparent simplicity, Richtmyer-Meshkov turbulent mixing zones are challenging flows to model. The main reason is that they obey the principle of permanence of large-eddies so that initial conditions have a lasting influence on their evolution.

The main purpose of this work was to account for this initial condition dependency in a Langevin PDF model. To this end, we considered the two-scale methodology usually considered for Reynolds stress models [32] and adapted it to the simplified Langevin model (SLM). As a result, we derived a two-scale Langevin model. Its large scale part accounts for the preservation of large scale initial conditions, while its small scale part is similar to the usual SLM.

In addition to this aspect, we also discussed the role played by the turbulent transport by the pressure flux. The latter is almost systematically neglected in Langevin models, while it may play a role in a mixing zone. A closure for this term was thus proposed.

The two-scale Langevin model, with a pressure flux term, was validated by comparing it against several LES of Richtmyer-Meshkov turbulent mixing zones. In these simulations, the initial conditions were varied in order to obtain different self-similar states. As a whole, the proposed model yields results which are in good agreement with the LES. The mixing zone width, levels of kinetic energy and anisotropy are correctly reproduced. Besides, the shapes of the modeled PDF are also coherent with those extracted from the LES. On all of these aspects, the proposed model offers a significant improvement over the standard SLM.

As a perspective, the precise formulation of the proposed model is tightly tied to the properties of Richtmyer-Meshkov turbulent mixing zones. However, the overall methodology which allowed to derive this model can be used in other contexts. Besides, as for Reynolds stress models [32], two-scale formulations with broader range of applications can also in principle be adapted from the present methodology.

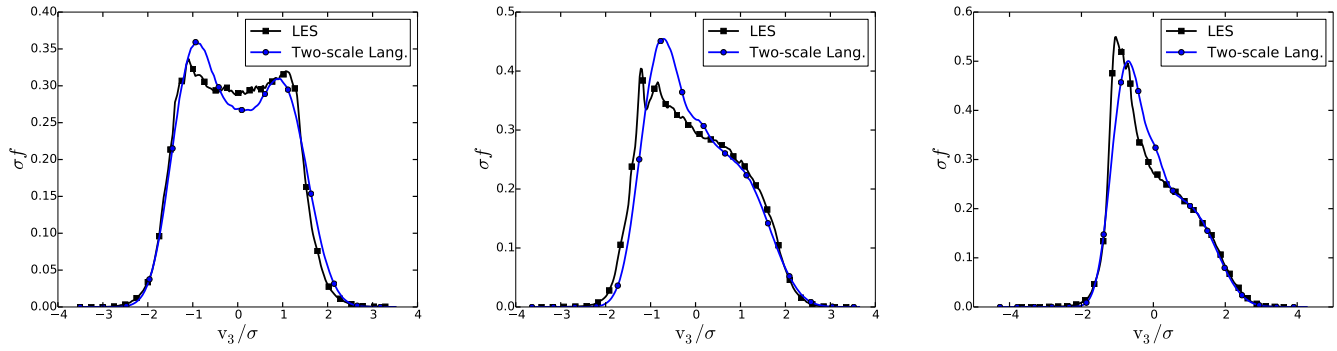

$x_3/L_k \approx 0$ $x_3/L_k \approx 0.2$ $x_3/L_k \approx 0.4$

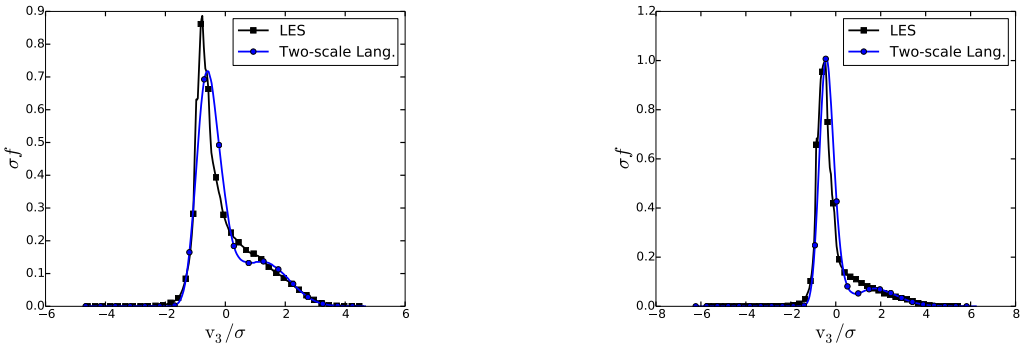

$x_3/L_k \approx 0.6$ $x_3/L_k \approx 0.8$

Figure 8: PDF of the longitudinal velocity at different points and at the end of the simulation with $s_0 = 1$.

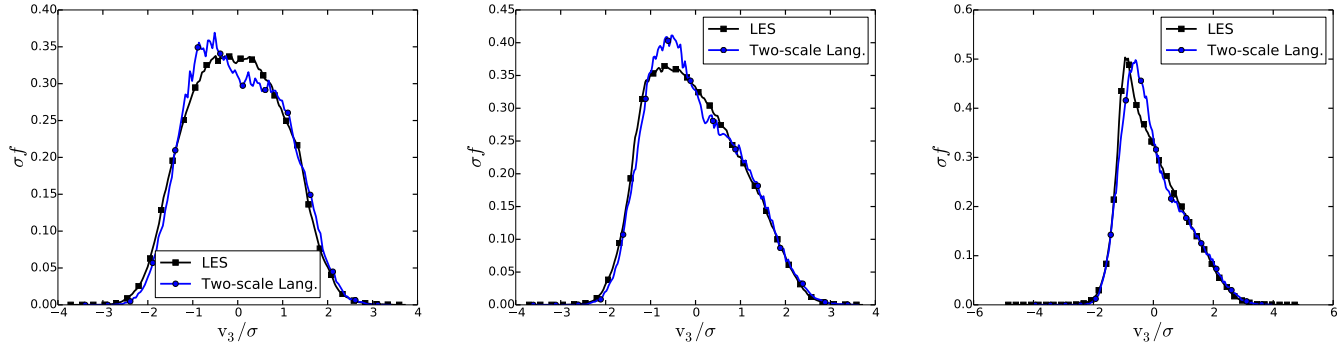

$x_3/L_k \approx 0$ $x_3/L_k \approx 0.2$ $x_3/L_k \approx 0.4$

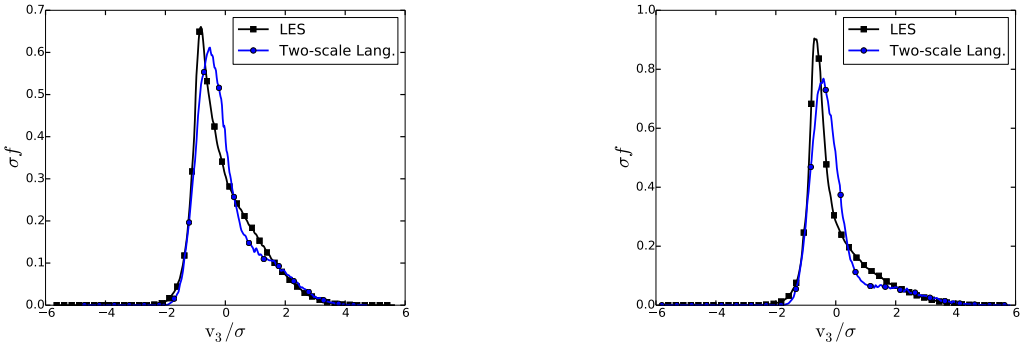

$x_3/L_k \approx 0.6$ $x_3/L_k \approx 0.8$

Figure 9: PDF of the longitudinal velocity at different points and at the end of the simulation with $s_0 = 2$.

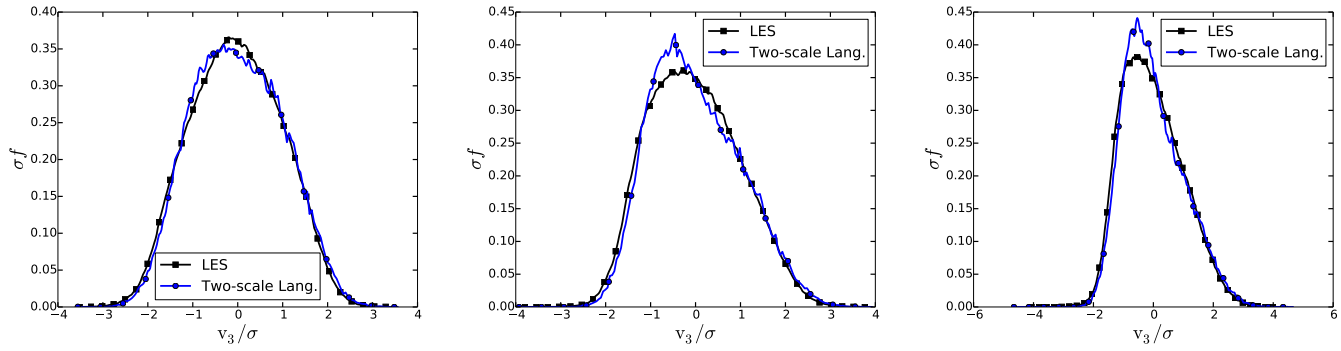

$x_3/L_k \approx 0$ $x_3/L_k \approx 0.2$ $x_3/L_k \approx 0.4$

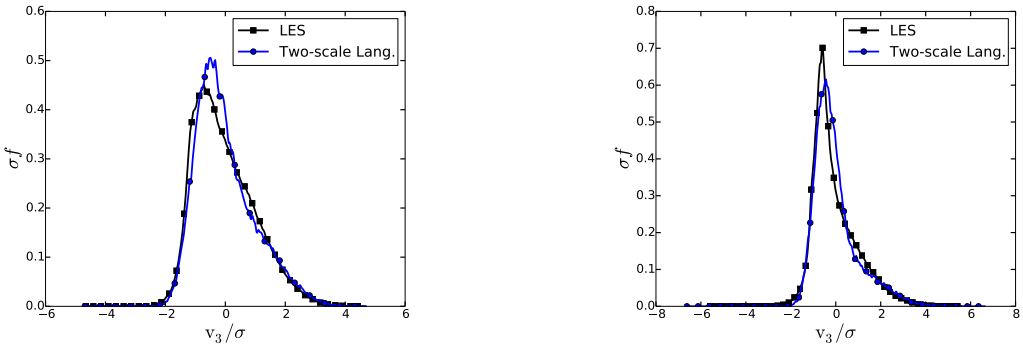

$x_3/L_k \approx 0.6$ $x_3/L_k \approx 0.8$

Figure 10: PDF of the longitudinal velocity at different points and at the end of the simulation with $s_0 = 3$.

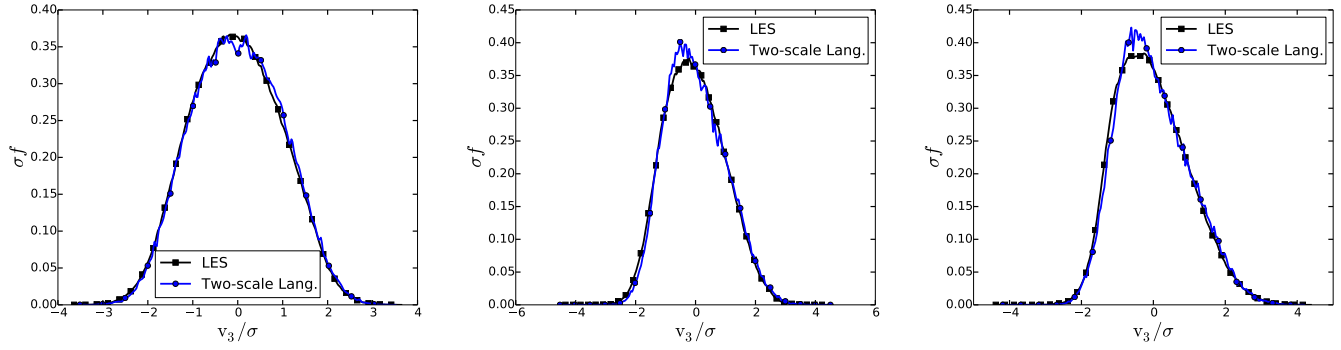

$x_3/L_k \approx 0$ $x_3/L_k \approx 0.2$ $x_3/L_k \approx 0.4$

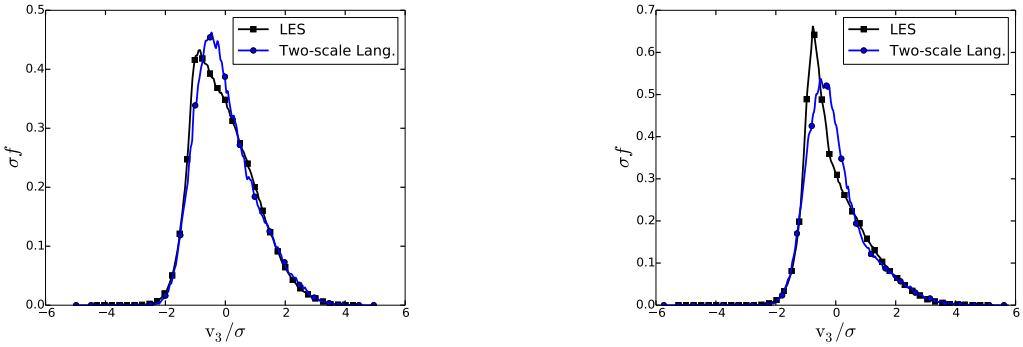

$x_3/L_k \approx 0.6$ $x_3/L_k \approx 0.8$

Figure 11: PDF of the longitudinal velocity at different points and at the end of the simulation with $s_0 = 4$.

References

[1] R. Richtmyer, Taylor instability in shock acceleration of compressible fluids, Comm. Pure. Appl. Math. 13 (1960) 297–319.

[2] E. Meshkov, Instability at the interface of two gases accelerated by a shock wave, Fluid Dyn. 43 (5) (1969) 101–104.

[3] M. Brouillette, The Richtmyer-Meshkov instability, Ann. Rev. Fluid Mech. 34 (1) (2002) 445–468.

[4] Y. Zhou, Rayleigh–Taylor and Richtmyer–Meshkov instability induced flow, turbulence, and mixing. i, Phys. Rep. 720-722 (2017) 1–136.

[5] Y. Zhou, Rayleigh–Taylor and Richtmyer–Meshkov instability induced flow, turbulence, and mixing. ii, Phys. Rep. 723-725 (2017) 1–160.

[6] T. Oggian, D. Drikakis, D. Youngs, R. Williams, Computing multi-mode shock induced compressible turbulent mixing at late times, J. Fluid Mech. 779 (2015) 411–431.

[7] O. Soulard, J. Griffond, D. Souffland, Pseudocompressible approximation and statistical turbulence modeling: Application to shock tube flows, Phys. Rev. E 85 (2012) 026307.

[8] J. Chasnov, On the decay of inhomogeneous turbulence, J. Fluid. Mech 342 (1997) 335–354.

[9] N. Inogamov, The role of Rayleigh–Taylor and Richtmyer–Meshkov instabilities in astrophysics: an introduction, Astrophys. Space. Phys. 10 (1999) 1–335.

[10] D. Youngs, Effect of initial conditions on self-similar turbulent mixing, in: IWPCTM-9, 2004, available online at: http://www.iwpctm.org.

[11] B. Thornber, D. Drikakis, D. L. Youngs, R. J. R. Williams, The influence of initial conditions on turbulent mixing due to Richtmyer–Meshkov instability, J. Fluid Mech. 654 (2010) 99–139.

[12] A. Llor, Invariants of free turbulent decay, arXiv/physics 0612220 (2006).

[13] O. Soulard, F. Guillois, J. Griffond, V. Sabelnikov, S. Simoëns, Permanence of large eddies in richtmyer-meshkov turbulence with a small atwood number, Phys. Rev. Fluids 3 (2018) 104603.

[14] L. Loitsyanskii, Some basic laws of isotropic turbulent flow, Trudy Tsentr. Aero.-Giedrodin. Inst. 440 (1939) 3–23.

[15] A. Kolmogorov, On the degeneration of isotropic turbulence in an incompressible viscous fluid, Dokl. Akad. Nauk. SSSR 31 (1941) 538–541.

[16] L. D. Landau, E. M. Lifshitsz, Continuum mechanics, Gostekhizdat, Moscou, 1954.

[17] P. Saffman, The large-scale structure of homogeneous turbulence, J. Fluid Mech. 27 (3) (1967) 581–593.

[18] A. Llor, Langevin equation of big structure dynamics in turbulence, Eur. J. Mech. B 30 (5) (2011) 480–504.

[19] P. Davidson, Turbulence: an introduction for scientists and engineers, Oxford University Press, Oxford, UK, 2004.

[20] M. Lesieur, Turbulence in fluids, 4th Edition, Springer, 2008.

[21] M. Lesieur, S. Ossia, 3D isotropic turbulence at very high Reynolds numbers: EDQNM study, J. Turb 1 (2000) 1–25.

[22] V. Mons, J.-C. Chassaing, T. Gomez, P. Sagaut, Is isotropic turbulence decay governed by asymptotic behavior of large scales ? an eddy-damped quasi-normal Markovian-based data assimilation study, Phys. Fluids 26 (2014) 115105.

[23] J. Chasnov, The decay of axisymmetric homogeneous turbulence, Phys. Fluids 7 (1995) 600–605.

[24] P. Davidson, N. Okamoto, Y. Kaneda, On freely decaying, anisotropic, axisymmetric saffman turbulence, J. Fluid Mech. 706 (2012) 150–172.

[25] V. Mons, M. Meldi, P. Sagaut, Numerical investigation on the partial return to isotropy of freely decaying homogeneous axisymmetric turbulence, Phys. Fluids 26 (2014) 025110.

[26] S. B. Pope, PDF methods for turbulent reactive flows, Prog. Energ. Combust. 27 (1985) 119–192.

[27] S. B. Pope, Turbulent flows, Cambridge Univ. Press, 2000.

[28] S. Pope, On the relationship between stochastic Lagrangian models of turbulence and second-moment closures, Phys. Fluids 6 (1994) 973–985.

[29] P. Van Slooten, Jayesh, S. Pope, Advances in PDF modeling for inhomogeneous turbulent flows, Phys. Fluids 10 (1) (1998) 246–265.

[30] A. Yoshizawa, Statistical analysis of mean-flow effects on the pressure-velocity correlation, Phys. Fluids 14 (5) (2002) 1736–1744.

[31] D. Souffland, O. Grégoire, S. Gauthier, R. Schiestel, A two-time scale model for turbulent mixing flows induced by Rayleigh–Taylor and Richtmyer–Meshkov instabilities, Flow. Turb. Comb. 69 (2003) 123–160.

[32] R. Schiestel, Modélisation et simulation des écoulements turbulents, Hermes, 1993.

[33] R. O. Fox, The spectral relaxation model of the scalar dissipation rate in homogeneous turbulence, Phys. Fluids 7 (5) (1995) 1082–1094.

[34] G. Barenblatt, Self-similar turbulence propagation from an instantaneous plane source,, Nonlinear Dynamics and Turbulence (1983) 48–60.

[35] J. Ramshaw, Simple model for linear and non-linear mixing at unstable fluid interfaces with variable acceleration, Phys. Rev. E 58 (1998) 5834–5840.

[36] V. R. Kuznetsov, On velocity difference probability density (PDF) at two points of a homogeneous, isotropic turbulent flow, PMM 31 (6) (1967) 1069–1072.

[37] V. R. Kuznetsov, V. A. Sabel'nikov, Turbulence and Combustion, Hemisphere Publishing Corporation, London, 1990.

[38] A. Llor, Statistical hydrodynamics models for developped instability flows, Vol. 681 of Lect. Notes Phys., Springer, Berlin Heidelberg, 2005.

[39] S. Pope, Simple models of turbulent flows, Phys. Fluids 23 (2011) 011301.

[40] B. Launder, B. Reece, W. Rodi, Progress in the development of a Reynolds-stress turbulence closure, J. Fluid. Mech. 68 (3) (1975) 537–566.

[41] O. Grégoire, D. Souffland, S. Gauthier, A second-order turbulence model for gaseous mixtures induced by Richtmyer-Meshkov instabilities, J. of Turbulence 6 (29) (2005).

[42] J. Lumley, Pressure strain correlation, Phys. Fluids 18 (1975) 750.

[43] N. Mansour, J. Kim, P. Moin, Reynolds-stress and dissipation rate budgets in a turbulent channel flow, Tech. Rep. 89451, NASA (December 1987).

[44] J. Groth, Description of the pressure in the reynolds strress transport equation, Phys. Fluids A 3 (9) (1991) 2276–2277.

[45] A. Burden, The influence of pressure fluctuations on double velocity correlations, App. Sci. Res. 51 (1993) 489–494.

[46] S. Kim, M. Chung, Roles of pressure transport and intermittency for computation of turbulent free shear flows, Int. J. Heat Fluid Flow 16 (1995) 194–201.

[47] K. Suga, Improvement of second moment closure for turbulent obstacle and heat transfer, Int. J. Heat and Fluid Flow 25 (2004) 776–784.

[48] T. Craft, B. Launder, A Reynolds stress closure designed for complex geometries, Int. J. Heat Fluid Flow 17 (1996) 245–254.

[49] J. Lumley, Computational modeling of turbulent flows, Adv. Appl. Mech. 18 (1978) 123–176.

[50] I. Vallet, Reynolds stress modeling of three-dimensional secondary flows with emphasis on turbulent diffusion closure, J. App. Mech. 74 (2007) 1142–1155.

[51] S. Shanmuganathan, D. Youngs, J. Griffond, B. Thornber, R. Williams, Accuracy of high-order density-based compressible methods in low Mach vortical flows, Int. J. Numer. Meth. Fluids (2013) DOI: 10.1002/fld.3853.

[52] R. LeVeque, Finite Volume Methods for Hyperbolic Problem, CUP, 2002.

[53] V. Daru, C. Tenaud, High order one-step monotonicity-preserving schemes for unsteady compressible flow calculations, J. Comp. Phys. 193 (2004) 563–594.

[54] F. Guillois, Simulation of a turbulent mixing zone resulting from the richtmyer-meshkov instability using a probability density function model : Analysis of the turbulent kinetic energy trans-

port, Ph.D. thesis, cole centrale de Lyon – LMFA (Sept. 2018).
[55] C. Emako, V. Letizia, N. Petrova, R. Sainct, R. Duclous, O. Soulard, Diffusion limit of the simplified Langevin PDF model in weakly inhomogeneous turbulence, ESAIM Proc. Surv. 48 (2015) 400–419.